



Semnan University

Mechanics of Advanced Composite Structures

journal homepage: <http://MACS.journals.semnan.ac.ir>

Experimental and Numerical Investigation of Reinforcement Sheet Effect on the Bending Strength of Corrugated Composite Panels

A. Hemmatian Soorki ^a, A. Kabiri Ataabadi ^{b*}, M. Loh-Mousavi ^a

^a Department of Mechanical Engineering, Khomeinishahr Branch, Islamic Azad University, Khomeinishahr, Isfahan, Iran

^b Department of Mechanical Engineering, Malek Ashtar University of Technology, Iran

KEYWORDS

Corrugate
Composite
Three-point bending
Failure

ABSTRACT

This paper investigates the influence of reinforcement sheet on the bending strength of corrugated composite panel by numerical and experimental analysis based on three-point bending tests in both longitudinal and transverse directions. In the numerical analysis, Hashin failure criterion was used to detect the failure, and an instantaneous material properties degradation model via a VUSDFLD subroutine developed in the commercial software ABAQUS was employed to simulate the behavior of the panel after damage initiation. At first, the adequate position of the reinforcement sheet, which improved bending strength of the panel, is discovered among some proposed positions by numerical analysis. Then, the desired panel with optimum reinforcement sheet as an improved panel and a panel without the reinforcement sheet as a base panel were investigated by numerical and experimental analyses and the results were compared with each other. The results showed that for the longitudinal direction, adding a reinforcement sheet has an unfavorable effect on the bending strength to weight ratio of the panel, but for the transverse direction, it increases the bending strength to weight ratio significantly. Furthermore, the experimental results demonstrate that using Balsa wood as a core in the corrugated panels also leads to increasing the bending strength to weight ratio. All in all, it can be found from finite element analysis that the VUSDFLD subroutine is adequate for quick damage analysis with acceptable accuracy.

1. Introduction

Over the last decades, extensive researches have been carried out on the corrugated-sandwich composite panels. The purpose of these studies has generally been to optimize the core angle, the thickness of the shell, the core, the strength to weight ratio, the length of the bond between the face and the core, and the geometry of the core. Knox [1] used both experimental techniques and numerical analyses to investigate the structural performance of adhesively bonded steel corrugated core sandwich beam elements in bending transverse to the corrugations, under both static and fatigue loading. The results indicated that the performance depends on the relative dimensions of the core and the face plate materials. Zhang [2] considered fiber type, corrugation angle, core-sheet thickness, the bond length between core and face-sheets, and foam inserts as the key design parameters to

explore novel designs of lightweight load-bearing structures which can absorb the energy in vehicles. Liu et.al [3] investigated the effect of a shock absorber on low-velocity impact behavior of sandwich structures with a corrugated core by using empirical studies as well as numerical simulations. Furthermore, investigations by Han [4] showed that filling the corrugated steel sandwich core with the polymer foam results in increasing the transverse shear strength even under equal mass conditions. Moreover, numerical and experimental investigations of sandwich panels with hybrid honeycomb core and corrugated metal sheet exposed to out-of-plane compression, transverse shear, and three-point bending by Han [5] led to achieving significant enhancement in strength and energy absorption in this sandwich panel compared to a hollow core corrugated ones. Paczos et.al [6] investigated some geometrical parameters in a five-layer orthotropic corrugated sandwich

* Corresponding author. Tel.: 031-45914544, Fax: 03145368955, ORCID ID: [0000-0002-6406-6928](https://orcid.org/0000-0002-6406-6928)
E-mail address: a.kabiri.at@mut-es.ac.ir

beam numerically and experimentally under the three-point bending load. Schneider [7] studied the effect of mass distribution on maximum load and energy absorption of corrugated sandwich panels made of self-reinforcing polyethylene terephthalate. In addition, Yu et.al [8] examined the failure modes and critical load for adhesively bonded steel corrugated sandwich panels under the three-point bending load experimentally, numerically and analytically. Liu et.al [9] inspected the mechanical behavior of the Y-frame sandwich core fabricated from carbon fiber reinforced polymer composite using the three-point bending test. The results revealed that the bending properties of the Y-frame sandwich core were strongly influenced by the relative density. Soltani [10] studied the geometrically nonlinear behavior of corrugated laminated composite shells (CLCS) under quasi-static loading along the corrugated direction experimentally and numerically. Li [11] investigated the three-point bending properties of bi-directional corrugated lattice sandwich structures fabricated from jute fibers and epoxy resin in order to explore the various modes of failure, destruction processes, and mechanical properties. Experimental results show that failure mainly occurs via three modes: face sheet crushing, face sheet wrinkling, and core member crushing. Furthermore, the simulation results were in good agreement with the experimental ones so that the relative errors of displacement and load are all within 20 %. In another experiment, Daliri [12] proposed a bidirectional sinusoidal corrugated core panel and studied the influence of the number of waves on the flexural properties of the panels with bi-directional or regular corrugated cores. The results show that the specific energy absorption of the novel corrugated core panels is improved compared to the regular core with the transverse arrangement. Jiang [13], also, proposed a horizontal stiffener to efficiently reinforce the flexural performances of corrugated core SCS by FEM. To design better structural parameters of stiffener, the effects of the stiffener thickness, position, and number on flexural behaviors of SCS are predicted in accordance with the finite element (FE) method. He concluded that the mechanical behaviors of any SCS are clearly reflected by four stages including elastic deflection, matrix cracking/fiber fracture, ductile damage/core deformation and stable deformation. Han [14] created a combined experimental-numerical approach to characterize the strength degradation of the adhesively bonded corrugated sandwich beam in hostile hot-humid environment. The experimental results in that study revealed that exposure in aqueous environment introduced

significant degradation in the structural peak load and energy absorption properties. Indeed, he found good agreement between numerical and experimental results. Farrokhhabadi [15] investigated mechanical behavior of multilayer corrugated core laminated composite sandwich panel subjected to quasi-static three-point bending both experimentally and numerically. Parameters such as contact force, energy absorption and specific absorbed energy (unit mass energy) for different geometries of corrugated core (rectangular, trapezoidal and triangular) were examined during loading process and failure. He noticed that using the multilayer method leads to the enhancement of peak loads as well as the extension of the vibratory area of the load-displacement diagram, whereas the amount of absorbed energy in comparison to nonreinforced specimen increases consequently.

Zangana [16] hybridized trapezoidal corrugated core glass-fibre sandwich structures using Kevlar and Zylon fibres to improve the dynamic impact performance. The impact behavior, damage mode, specific absorbed energy, and residual strength after the impact of the composite sandwiches were investigated administering a low-velocity impact test. The obtained experimental results showed that the hybridized sandwiches with high-performance fibre are performing extremely well when subjected to impact energy above the threshold limit. As a matter of fact, employing high-performance ply in the sandwich core provided high specific energy absorption without increasing structural weight.

In this paper, the influence of the reinforcement sheet on the strength of a corrugated composite sandwich panel was investigated experimentally and numerically under three-point bending load. In order to find the best location of the reinforcement sheet, numerical analysis was done via ABAQUS for three various locations of the reinforcement sheet. A VUSDFLD subroutine was used to consider the reduction of material properties due to the failure. After finding the best location of the reinforcement sheet, the desirable models, as well as the model without reinforcement, were also investigated experimentally and the results were discussed.

2. Damage model

Wei [17] employed a 3D Hashin damage criterion to investigate the behavior of a composite plate with a central hole. He simulated the progressive damage in the plate applying the 3D Hashin damage criterion and material properties degradation approach. 3D

Hashin damage criterion used in VUSDFLD subroutine is as follow [17]:

Tensile failure in warp direction ($\sigma_1 > 0$):

$$\left(\frac{\sigma_1}{X_T}\right)^2 + \left(\frac{\tau_{12}}{S_{12}}\right)^2 + \left(\frac{\frac{\tau_{31}^2}{2G_{31}} + \frac{3}{4}\alpha\tau_{31}^4}{\frac{S_{31}^2}{2G_{31}} + \frac{3}{4}\alpha S_{31}^4}\right)^2 \geq 1 \quad (1)$$

Compressive failure in warp direction ($\sigma_1 < 0$):

$$\left(\frac{\sigma_1}{X_C}\right)^2 \geq 1 \quad (2)$$

Tensile failure in weft direction ($\sigma_2 > 0$):

$$\left(\frac{\sigma_2}{Y_T}\right)^2 + \left(\frac{\tau_{12}}{S_{12}}\right)^2 + \left(\frac{\frac{\tau_{23}^2}{2G_{23}} + \frac{3}{4}\alpha\tau_{23}^4}{\frac{S_{23}^2}{2G_{23}} + \frac{3}{4}\alpha S_{23}^4}\right)^2 \geq 1 \quad (3)$$

Compressive failure in weft direction ($\sigma_2 < 0$):

$$\left(\frac{\sigma_2}{Y_C}\right)^2 \geq 1 \quad (4)$$

Tensile failure in normal direction ($\sigma_3 > 0$):

$$\left(\frac{\sigma_3}{Z_T}\right)^2 + \left(\frac{\frac{\tau_{31}^2}{2G_{31}} + \frac{3}{4}\alpha\tau_{31}^4}{\frac{S_{31}^2}{2G_{31}} + \frac{3}{4}\alpha S_{31}^4}\right)^2 + \left(\frac{\frac{\tau_{23}^2}{2G_{23}} + \frac{3}{4}\alpha\tau_{23}^4}{\frac{S_{23}^2}{2G_{23}} + \frac{3}{4}\alpha S_{23}^4}\right)^2 \geq 1 \quad (5)$$

Compressive failure in normal direction ($\sigma_3 < 0$):

$$\left(\frac{\sigma_3}{Z_C}\right)^2 + \left(\frac{\frac{\tau_{31}^2}{2G_{31}} + \frac{3}{4}\alpha\tau_{31}^4}{\frac{S_{31}^2}{2G_{31}} + \frac{3}{4}\alpha S_{31}^4}\right)^2 + \left(\frac{\frac{\tau_{23}^2}{2G_{23}} + \frac{3}{4}\alpha\tau_{23}^4}{\frac{S_{23}^2}{2G_{23}} + \frac{3}{4}\alpha S_{23}^4}\right)^2 \geq 1 \quad (6)$$

In the above equations, X_T and X_C are strengths in the longitudinal (warp) or 1 direction. Y_T and Y_C are strengths in the transverse (weft) or 2 direction. Z_T and Z_C are strengths in the thickness or 3 direction and S is shear strength. The subscripts T and C refer to tension and compression. α is a material nonlinearity factor which is considered 3.057×10^{-8} MPa⁻³ [17].

Figure 1 depicted a flowchart of the VUSDFLD subroutine, the related parameters of which are introduced in Table.1. When failure occurs in any of the above modes, the mechanical properties are changed according to Table 2.

3. Materials and specimens

In the current research, in compliance with the composite corrugate sandwich panel fabricated, tested and analyzed by Schneider et.al [7] which has no reinforcement sheet, some specimens with a reinforcement sheet are

considered, and experimentally and numerically investigated under bending load in both longitudinal and transverse directions as shown in Fig. 2. Figure 3 displays the base model cross-section dimensions for the longitudinal and transverse specimens, respectively. All dimensions are in millimeters. Figures 4 to 6 depict the dimensions of the longitudinal models with the reinforcement sheet introduced by symbols "A" to "C". The material properties of the various models are listed in Table 3. The specimens were made of E-glass woven textile, Resin Ec130, and W340 hardener.

Table 1. State variables used in the VUSDFLD subroutine.

Symbol	Description
SDV1	Warp failure
SDV2	Weft failure
SDV3	Matrix failure
SDV4	Tensile failure in warp direction
SDV5	Compressive failure in warp direction
SDV6	Tensile failure in weft direction
SDV7	Compressive failure in weft direction
SDV8	Tensile failure in normal direction

Table 2. State variables used in the VUSDFLD subroutine.

Symbol	Description
$E1^* = 0.1E1$; $G12^* = 0.1G12$; $G31^* = 0.1G31$; $\mu12^* = 0.1\mu12$; $\mu13^* = 0.1\mu13$;	Warp failure
$E2^* = 0.1E2$; $G12^* = 0.1G12$; $G23^* = 0.1G23$; $\mu12^* = 0.1\mu12$; $\mu23^* = 0.1\mu23$;	Warp failure
$E3^* = G31^* = G23^* = \mu31^* = \mu23^* = 0$	Matrix failure

Table 3. Material properties of the composite specimens with E-glass fibers, resin Ec130 and W340 hardener.

Symbol	Amount	Unit
XT	281	MPa
XC	170	MPa
YT	281	MPa
YC	170	MPa
ZT	58	MPa
ZC	84	MPa
S12	140	MPa
S23	29	MPa
S31	29	MPa
E1	14360	MPa
E2	14360	MPa
E3	3470	MPa
Nu12	0.26	-
Nu13	0.3	-
Nu23	0.3	-
G12	1735	MPa
G13	1334	MPa
G23	1334	MPa

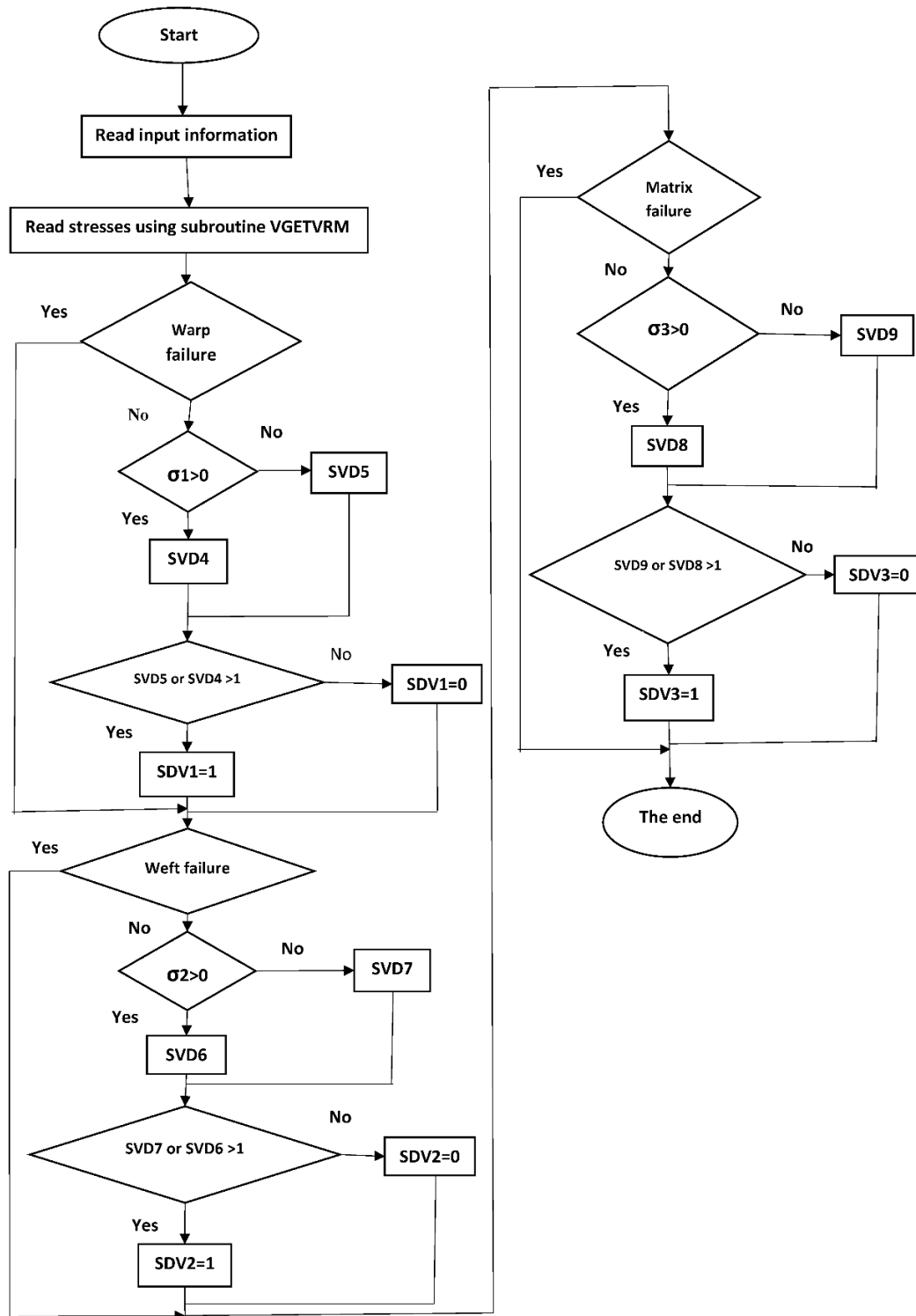


Fig. 1. Flowchart of the VUSDFLD subroutine used for damage analysis.

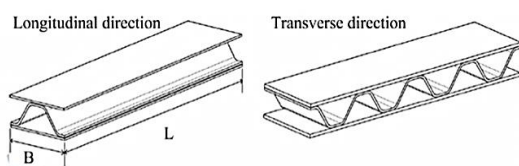


Fig. 2. Longitudinal and transverse directions of a corrugated sandwich panel composite without the reinforcement layer [8].

VUSDFLD subroutine was employed to consider material properties degradation of the composite during the three-point bending FE simulation. Simulating the corrugated panel with reinforcement layers was carried out based upon the properties of Table 4. The model was meshed by C3D8R elements. To obtain the proper position of the reinforcement layer, three

locations were considered according to Figs. 4 to 6, and the FE results of various models were compared with one another. The results are given in Table 4. Table 5 exhibits the variations of the volume and force for each model. Letters (L) and (T) denote the longitudinal and transverse models, respectively.

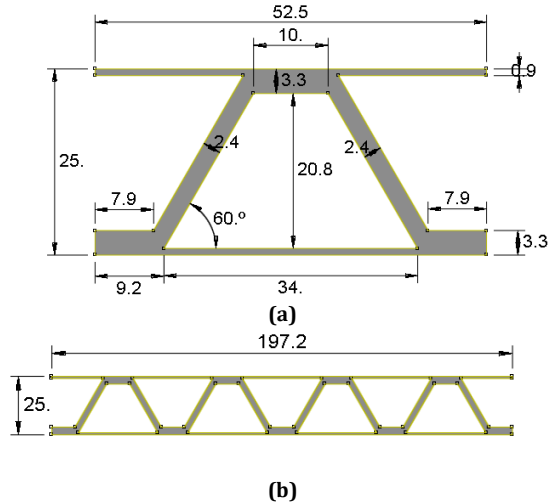


Fig. 3. Base model cross-section dimensions of (3-8-3) specimens without reinforcement sheet, (a) longitudinal specimens and (b) transverse specimens.

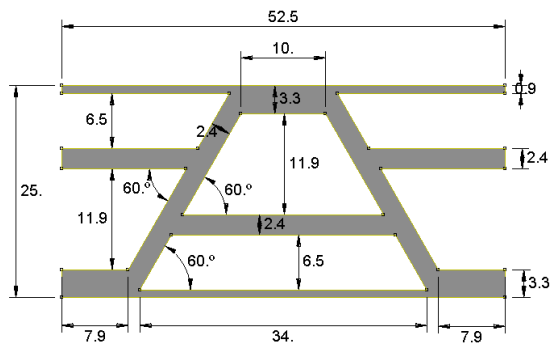


Fig. 4. Cross-section dimensions of (3-8-3) model with reinforcement layer in the longitudinal mode introduced by symbol "A".

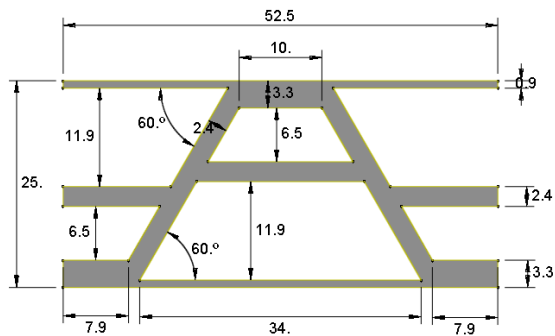


Fig. 5. Cross-section dimensions of (3-8-3) model with reinforcement layer in the longitudinal mode introduced by symbol "B".

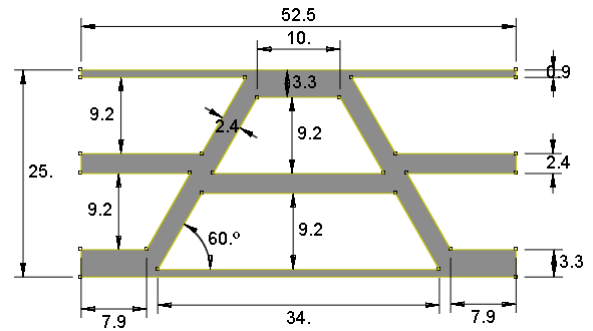


Fig. 6. Cross-section dimensions of (3-8-3) model with reinforcement layer in the longitudinal mode introduced by symbol "C".

Table 4. Material properties of the composite specimens with E-glass fibers, resin Ec130 and W340 hardener.

Symbol	Amount	Unit
XT	281	MPa
XC	170	MPa
YT	281	MPa
YC	170	MPa
ZT	58	MPa
ZC	84	MPa
S12	140	MPa
S23	29	MPa
S31	29	MPa
E1	14360	MPa
E2	14360	MPa
E3	3470	MPa
Nu12	0.26	-
Nu13	0.3	-
Nu23	0.3	-
G12	1735	MPa
G13	1334	MPa
G23	1334	MPa

According to the results, it can be found that the model "A" has the highest strength-to-weight ratio in comparison with the others. Therefore, the model "A" was picked as the best model to be manufactured and investigated numerically and experimentally.

4. Manufacturing and three-point bending test

In this study, the hand layup method was employed to manufacture the specimens. Balsa wood was utilized to build the core mold of the specimens. The wood molds were polished with soft grind sheet, lubricated with oil and covered with thin plastic in order to ensure that the models can be easily removed from the core. Figure 7 shows the stages of preparing the Balsa wood core molds.

To manufacture the composite specimens, EC130 resin, W340 hardener and 200 gr woven E-glass fiber in [0, 90] stacking sequence were utilized. Figure 8 depicts the construction of the template without any reinforcement sheet.

Table 5. Geometrical characteristics of the specimens





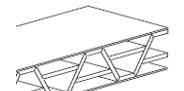
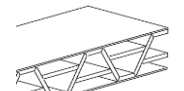
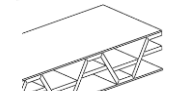
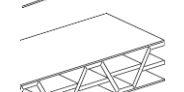
Corrugated Model		Max. Amount		Weft failure		Warp failure		Matrix failure	
		Displacement (mm)	Force (N)	Displacement (mm)	Force (N)	Displacement (mm)	Force (N)	Displacement (mm)	Force (N)
3D-Solid-Horizontal Support-3-8-3-A-L		3.3	4119	1.32	1455	1.26	1928	0.66	1076
3D-Solid-Horizontal Support-3-8-3-B-L		3.41	4250	1.32	1883	1.26	1462	0.72	1054
3D-Solid-Horizontal Support-3-8-3-C-L		3.24	3835	1.32	1805	1.26	1960	0.72	1025
3D-Solid-Without Support-3-8-3-L		3.3	3727	1.26	1724	1.26	1724	0.66	1020
3D-Solid-Horizontal Support-3-8-3-A-T		3.91	2889	2.75	2121	2.71	2204	2.75	2121
3D-Solid-Horizontal Support-3-8-3-B-T		3.71	2045	2.03	1385	2.03	1385	2.03	1385
3D-Solid-Horizontal Support-3-8-3-C-T		4.68	2835	2.64	2030	2.64	2030	2.64	2030
3D-Solid-Without Support-3-8-3-T		1.53	1332	2.06	770	2.06	770	2.06	770

Figure 9 illustrates the steps of building the specimen with the reinforcement sheet. To have 8 layers in each part of the sandwich corrugate, at first, 4 layers are put around the circumference of Balsa wood which is the smaller core. In the next stage, after arranging down area of the core, Balsa wood which is bigger core is put on it and then 4 layers are arranged on the core again. In the next stage, the smaller prepared core is put on the bigger one. Finally, 4 layers are put on them and the sandwich corrugate with 8 layers on each face is manufactured.





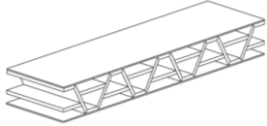
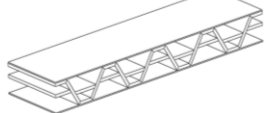
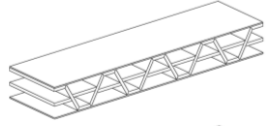

After preparing the specimens, they were put on the vacuum table. The specimens were vacuumed under pressure of -0.6 bar for 4 hours at 21 ° C. After 4 hours, the vacuum pump was

turned off and the specimens were completely dried after 24 hours. The prepared specimens were cut to the desired size. Figure 10 shows the vacuum process. Various views of the specimens are shown in Fig. 11, as well.

Figs. 12 and 13 show the specimens for the bending test which were prepared with and without the reinforcement sheet in longitudinal and transverse directions, respectively.

The bending test was carried out by HOUNSFIELD machine with a load range of 25 kN, an accuracy of 1 kN, a 50 kN nominal capacity of load cell, and a roller diameter of 50 mm. The moving speed of jaws was considered 2 mm/min. Figure 14 displays the specimens under the three-point bending test.

Table 6. Volume and force for various locations of the reinforcement layer.

Corrugated Model		Numeral values		Percentage (%)	
		Area (mm ²)	Force (N)	Area	Force
3D-Solid-Horizontal Support-3-8-3-A-L		412	4119	+48	+10
3D-Solid-Horizontal Support-3-8-3-B-L		382	4250	+37.5	+14
3D-Solid-Horizontal Support-3-8-3-C-L		397	3835	+43	+3
3D-Solid-Without Support-3-8-3-L		278	3728	Base case	Base case
3D-Solid-Horizontal Support-3-8-3-A-T		1565	2890	+48	+117
3D-Solid-Horizontal Support-3-8-3-B-T		1455	2045	+37.5	+53.5
3D-Solid-Horizontal Support-3-8-3-C-T		1513	2835	+43	+113
3D-Solid-Without Support-3-8-3-T		1058	1332	Base case	Base case

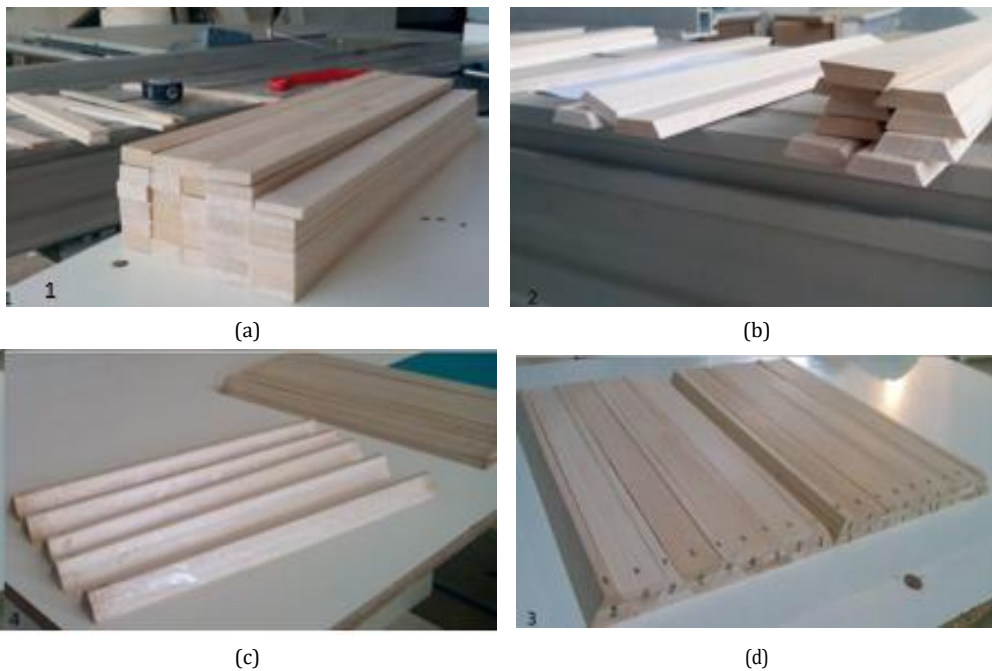
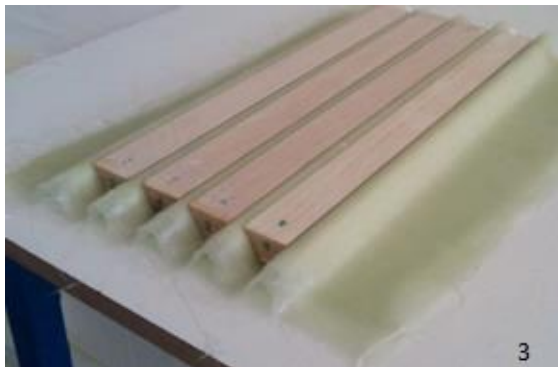


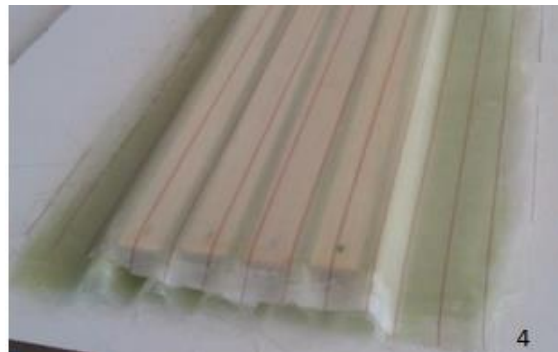
Fig. 7. Stages of preparing the Balsa wood core molds: (a) and (b) slicing the templates; (c) using plastic and lubricating it before composite layup; (d) final arranging the templates



(a)



(b)



(c)

Fig. 8. Steps of manufacturing the sandwich panel without reinforcement layer: (a) Putting three layers on the bottom and placing the core templates on it; (b) Putting the other core layers on the composite layers; (c) Putting three layers on the templates.

5. Experimental and numerical results

The rollers used in the three-point bending test were 25 mm in diameter and 60 mm in length. The distance between the two bottom rollers was 150 mm. Experiments and numerical analyses were done in four categories. Longitudinal and transverse specimens with and without reinforcement sheets were first manufactured and then investigated both experimentally and numerically. The results are discussed in detail in the subsequent sections.



(a)



(b)



(c)



(d)

Fig. 9. Manufacturing the specimen with reinforcement sheet: (a) Wrapping the four layers around the small core; (b) Putting the three layers below and placing the cores on it; (c) Putting the eight layers on the wrapped core; (d) The prepared templates which are ready for vacuum.



Fig. 10. Vacuum process of the prepared specimens.



Fig. 11. The manufactured specimens with initial cutting.

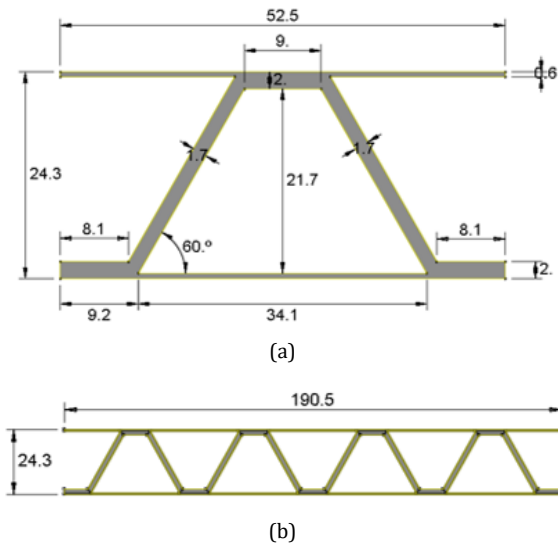


Fig. 12. Dimensions of the composite specimens without reinforcement sheet: (a) longitudinal; (b) transverse.

5.1. Longitudinal specimens without reinforcement sheet

Figure 15 depicts the load-displacement graph of the longitudinal specimens during the experimental and numerical analysis. As illustrated in the figure, the maximum loads for the first and second specimens which do not have Balsa core, are approximately close to the maximum load in numerical analysis. In the third specimen with a Balsa core, alongside increasing the specimen weight by 15%, the strength increases by 30% compared to the other two specimens. In the numerical analysis, after the final failure with the maximum load, an instantaneous reduction is observed in the graph which is due to the material properties degradation caused by VUSDFFD subroutine. In addition, it is worth noticing that the graph varies in a wavy manner since the friction was

taken into consideration. Figure 16 demonstrates the damage region developed in the specimens during the experiment compared to ones during the numerical analysis.

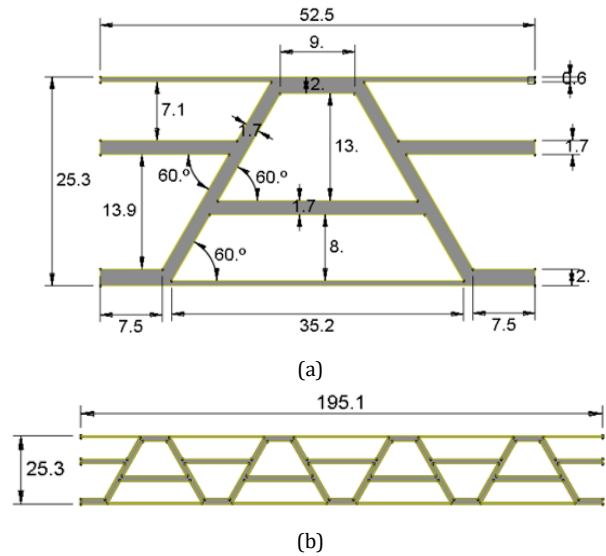


Fig. 13. Dimensions of the composite specimens with reinforcement sheet: (a) longitudinal; (b) transverse.



Fig. 14. HOUNSFIELD machine used for three-point bending test.

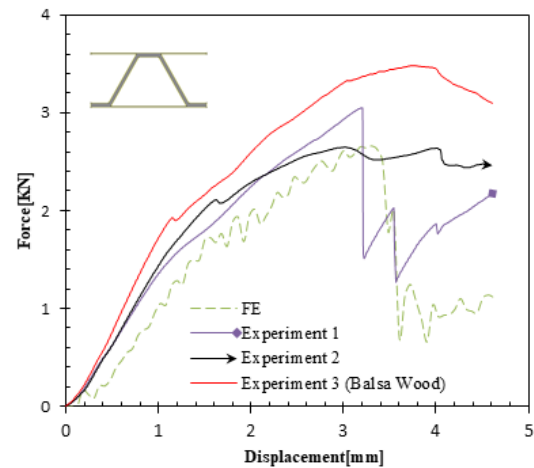


Fig. 15. Results of the experimental and numerical analysis for the longitudinal specimens without reinforcement sheet.

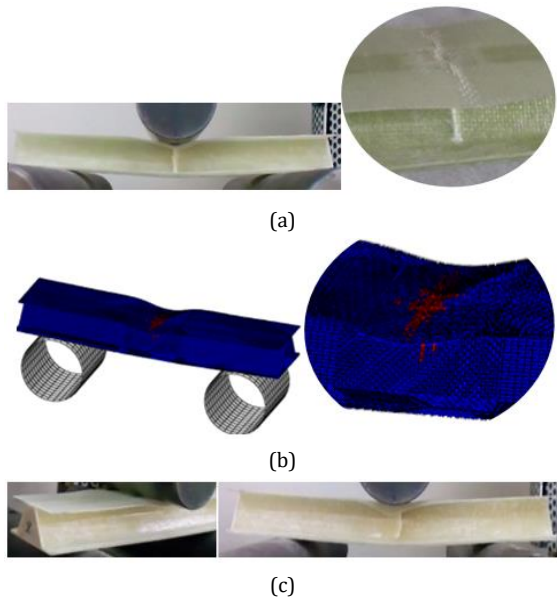


Fig. 16. Damage region developed in the longitudinal specimens without reinforcement sheet: (a) Experiment without Balsa wood; (b) FE simulation without Balsa wood; (c) Experiment with Balsa wood.

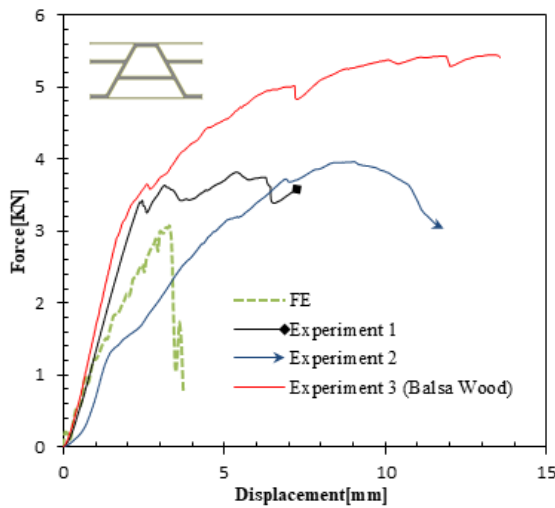


Fig. 17. Results of the experimental and the numerical analysis for the specimen with reinforcement sheet in the longitudinal case.

5.2. Longitudinal specimens with reinforcement sheet

Figure 17 shows the results of the experimental and the numerical analysis for the specimens with the reinforcement sheet in the longitudinal case. It seems that the lack of a fixture during manufacturing the specimens with a reinforcement sheet leads to more remainder of resin on the core walls, which leads to a difference in the load-displacement graph of the first and second specimens. In addition, this excessive resin makes the specimens heavier, and the experimental strengths are about 20% more than the

numerical one. As for the third specimen with a Balsa core, with %10 rise of the specimen weight, the strength grows by 30% compared to the other two specimens. Figure 18 shows damage region developed in the specimens during the experiment compared to the ones in the numerical analysis.

5.3. Transverse specimens without reinforcement sheet

In the first specimen after starting the bending process and bearing a little force, the top plate on one side was defeated. Due to the specimen slip on the device jaws, the bending test of the second was not accomplished properly. Figure 19 depicts the load-displacement graph related to the two specimens as well as the numerical analysis. Figure 20 exhibits the failure modes of the specimens without the reinforcement sheet in the transverse case. As it can be observed from the results, the acceptable agreement between numerical and experimental results is not achieved which can be due to slipping occurred in the test and the failure was happened from the asymmetric load applied on the specimens as shown in Fig. 20.

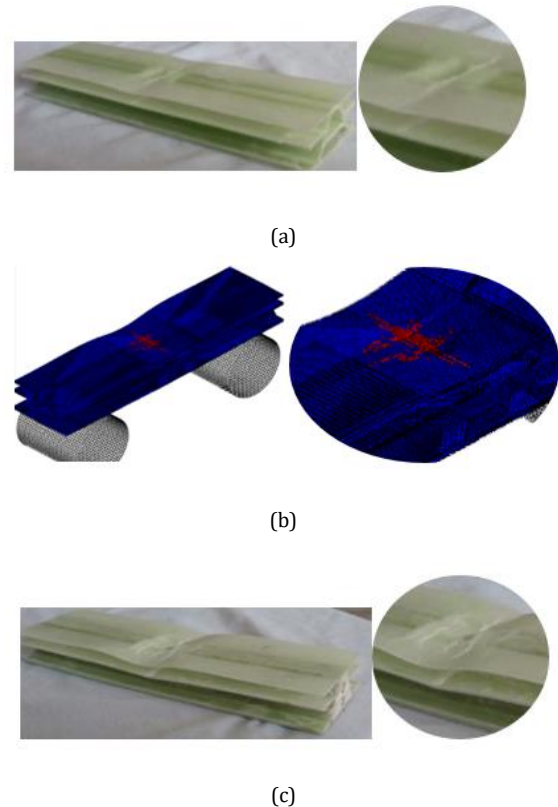


Fig. 18. Damage region developed in the longitudinal specimens with reinforcement sheet: (a) Experiment without Balsa wood; (b) FE simulation without Balsa wood; (c) Experiment with Balsa wood.

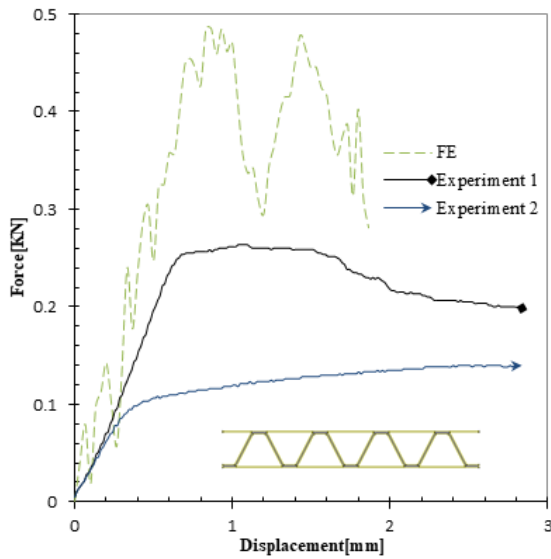


Fig. 19. Results of the experimental and the numerical analysis for the specimen without reinforcement sheet in the transverse case.

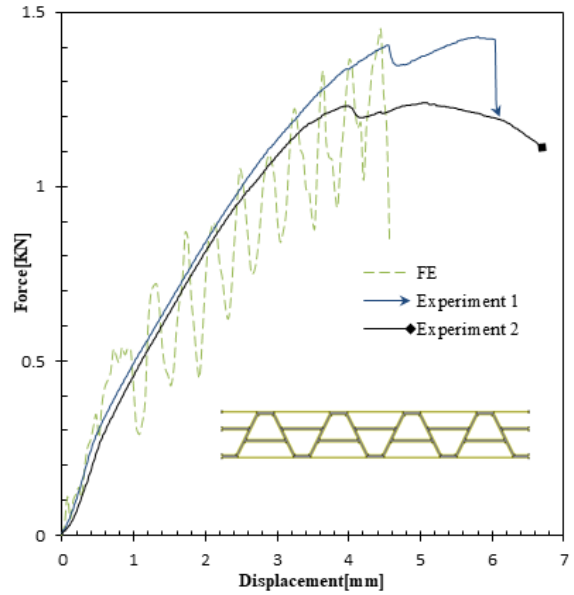


Fig. 21. Results of the experimental and the numerical analysis for the specimen with the reinforcement sheet in the transverse case.

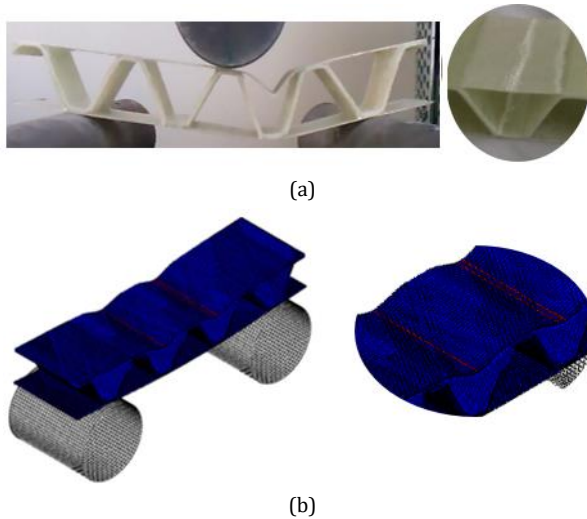


Fig. 20. Failure modes of the transverse specimens without the reinforcement sheet: (a) Experiment; (b) FE simulation.

5.4. Transverse model with reinforcement sheet

Figure 21 shows the load-displacement graph of the two specimens along with the numerical analysis. In the first experiment, the first failure is attributed to the splitting of the shell and the second failure is due to the breakdown of the core. In the second experiment, there is a minor difference compared to the first ones that can be related to breaking of the top plate as the bending occurs. The three curves are in good agreement and the ultimate bending strength is almost equal.

Figure 22 exhibits the failure modes of the specimens with reinforcement sheet in transverse case.

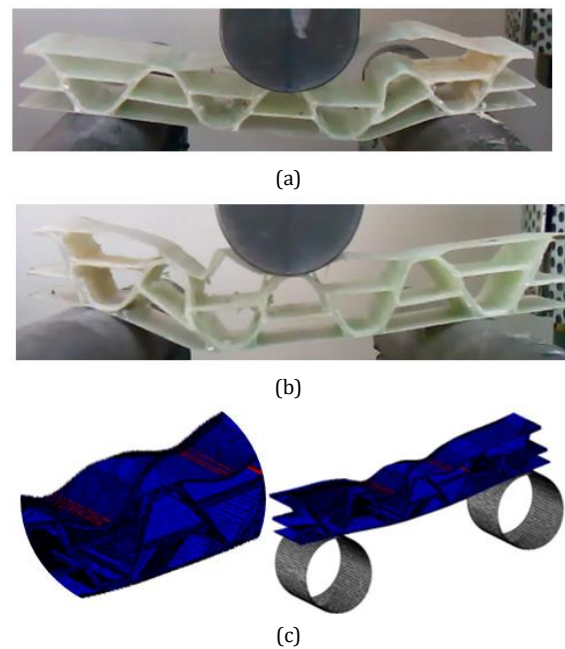


Fig. 22. Failure modes of the transverse specimens with the reinforcement sheet: (a) specimen 1; (b) specimen 2; (c) FE simulation.

6. Summary

Table 6 listed the summary of the experimental and numerical results of the panels with and without the reinforcement sheet in the longitudinal and transverse directions.

Table 7. Results of the experiments and numerical analysis.

Corrugated specimen	Test	Displacement (mm)	Force (N)	Weight (gr)	Force/Weight
3D-Solid-Horizontal Support 3-8-3-A-L	Test 1	5.39	3892	104	37.4
	Test 2	8.96			
	Test with Balsa wood	13.44	5445	122	44.6
	Simulation	3.3	3074	-	-
	Error (%)	-	21	-	-
	Test 1	3.2	2848	64	44.5
Test 2	3.02				
3D-Solid Without Support-3-8-3- L	Test with Balsa wood	3.78	3480	80	43.5
	Simulation	3.3	2666	-	-
	Error (%)	-	6.4	-	-
	Test 1	5.81	1335	97	13.8
Test 2	5.1				
3D-Solid-Horizontal Support-3-8-3-A-T	Simulation	4.44	1448	-	-
	Error (%)	-	8.5	-	-
	Test 1	1.1	202	61	3.8
Test 2	2.8				
3D-Solid-Without Support-3-8-3- T	Simulation	0.83	485	-	-
	Error (%)	-	140	-	-

7. Conclusions

This study aimed to shed light on the bending strength in the longitudinal and transverse directions of corrugated composite panel with and without the reinforcement sheet. Moreover, the effect of adding Balsa wood as a core of the panel was investigated. It needs to be highlighted that the specimens without the reinforcement sheet were considered as the basic panels. The obtained results verified that, in the longitudinal specimens, adding the reinforcement sheet led to improving the bending strength force while the specimen weight related to the based one was increased too. So the reinforcement sheet in the longitudinal specimens had an unfavorable effect on the bending strength to weight ratio of the panel. Without a doubt, it should be borne in mind that the reinforcement sheet had a minor positive effect on the results of the specimen when the Balsa wood was utilized as the core.

The results have also strengthened the conviction that that adding the reinforcement sheet in the longitudinal mode will be useful for a case in which there is no restriction on the weight. Unlike the longitudinal case, it is obvious that the addition of the reinforcement sheet in the transverse mode had an excellent effect (roughly three times) on the bending strength to the weight ratio. All in all, it can be concluded that adding the reinforcement sheet improves the performance of the corrugated panels against the bending loads in the transverse direction. Furthermore, the evidence from the finite element analysis points towards the idea that the VUSDFLD subroutine is adequate for quick damage analysis with acceptable accuracy. It should also be noted that the material properties are adopted from the design stages aviation industry, so they are conservative. This implies that the numerical results were below the experimental ones. Furthermore, the complexities in structure, modeling, boundary

conditions (contact) and the analysis of the damage could have resulted in discrepancies between the numerical and experimental results.

References

- [1] Knox, E.M., Cowling, M.J. and Winkle, I.E., 1998. Adhesively bonded steel corrugated core sandwich construction for marine applications. *Marine Structures*, 11, pp.185-204.
- [2] Zhang, J., Supernak, P., Mueller-Alander, S. and Wang, CH., 2013. Improving the bending strength and energy absorption of corrugated sandwich composite structure. *Mater. & Design*, 52, pp.767-773.
- [3] Liu, J., He, W., Xie, D. and Tao, B., 2017. The effect of impactor shape on the low-velocity impact behavior of hybrid corrugated core sandwich structures. *Composites Part B Engineering*, 111, pp.315-331.
- [4] Han, B., Bo, Y., Yu, X., Chang-Qing, C., Qian-Cheng, Z. and Jian, L.T., 2015. Foam filling radically enhances transverse shear response of corrugated sandwich plates. *Material & Design*, 77, pp.132-141.
- [5] Han, B., Wang, W., Zhang, Z., Zhang, Q., Jin, F. and Lu, T., 2016. Performance enhancement of sandwich panels with honeycomb-corrugation hybrid core. *Theoretical and Applied Mechanics Letters*, 6(1), pp.54-59.
- [6] Paczos, P., Wasilewicz, P. and Magnucka-Blandzi, E., 2016. Experimental and numerical investigations of five-layered trapezoidal beams. *Composite Structures*, 145, pp.129-141.
- [7] Schneider, C., Zenkert, D., Deshpande, V.S. and Kazemahvazi, S., 2016. Bending energy absorption of self-reinforced poly (ethylene terephthalate) composite sandwich beams. *Composite Structures*, 140, pp.582-589.
- [8] Yu, Y., Ying, L., Hou, W.B., Hu, P., Jia, X.X. and Akhmet, G., 2018. Failure analysis of adhesively bonded steel corrugated sandwich structures under three-point bending. *Composite Structures*, 184, pp.256-268.
- [9] Liu, J., He, Z., Liu, J. and Huang, W., 2019. Bending response and failure mechanism of composite sandwich panel with Y-frame core. *Thin-Walled Structures*, 145, 106387.
- [10] Soltani, Z., Hosseini Kordkheili, S.A. and Kress, G., 2019. Experimental and numerical study of geometrically nonlinear behavior of corrugated laminated composite shells using a nonlinear layer-wise shell FE formulation. *Engineering Structures*, 184, pp.61-73.
- [11] Li, S., Feng, Y., Qin, J., Li, S., Ye, G. and Hu, Y., 2019. Bending performance of a jute fiber and epoxy resin composite sandwich structure with a bi-directional corrugated truss core. *Fibers and Polymers*, 20, pp.2166-2174.
- [12] Daliri, V. and Zeinedini, A., 2019. Flexural behaviour of the composite sandwich panels with novel and regular corrugated cores. *Applied Composite Materials*, 26(3), pp.963-982.
- [13] Jiang, H., Ren, Y., Jin, Q., Zhu, G. and Liu, Z., 2019. Flexural performances of fiber face-sheets/corrugated core sandwich composite structures reinforced by horizontal stiffeners. *International Journal of Mechanical Sciences*, DOI: <https://doi.org/10.1016/j.ijmecsci.2019.105307>.
- [14] Han, X., Akhmet, G., Hu, P., Hou, W., Baubekov, Y. and Akhmetov, M., 2020. Numerical prediction on the mechanical degradation of adhesively bonded corrugated sandwich beam after hygrothermal ageing. *Composite Structures*, 241, DOI: <https://doi.org/10.1016/j.compstruct.2020.112131>.
- [15] Farrokhhabadi, A., Taghizadeh, S.A., Madadi, H., Norouzi, H. and Ataei, A., 2020. Experimental and numerical analysis of novel multi-layer sandwich panels under three point bending load. *Composite Structures*, DOI: <https://doi.org/10.1016/j.compstruct.2020.112631>
- [16] Zangana, S., Epaarachchi, J., Ferdous, W. and Leng, J., 2020. A novel hybridized composite sandwich core with Glass, Kevlar and Zylon fibres – Investigation under low-velocity impact. *International Journal of Impact Engineering*, 137, 103430.
- [17] Wei, W.G., 2014. Static tensile properties simulation of plane woven-reinforced laminates with hole damage. *Advanced Materials Research*, 936, pp.2017-2023.